Iron Overload and Diabetes Risk: A Shift From Glucose to Fatty Acid Oxidation and Increased Hepatic Glucose Production in a Mouse Model of Hereditary Hemochromatosis

Jingyu Huang,[1] Deborah Jones,[1] Bai Luo,[1] Michael Sanderson,[1] Jamie Soto,[1] E. Dale Abel,[1] Robert C. Cooksey,[1,2] and Donald A. McClain[1,2]

OBJECTIVE—Excess tissue iron levels are a risk factor for diabetes, but the mechanisms underlying the association are incompletely understood. We previously published that mice and humans with a form of hereditary iron overload, hemochromatosis, exhibit loss of β-cell mass. This effect by itself is not sufficient, however, to fully explain the diabetes risk phenotype associated with all forms of iron overload.

RESEARCH DESIGN AND METHODS—We therefore examined glucose and fatty acid metabolism and hepatic glucose production in vivo and in vitro in a mouse model of hemochromatosis in which the gene most often mutated in the human disease, *HFE*, has been deleted ($Hfe^{-/-}$).

RESULTS—Although $Hfe^{-/-}$ mice exhibit increased glucose uptake in skeletal muscle, glucose oxidation is decreased and the ratio of fatty acid to glucose oxidation is increased. On a high-fat diet, the $Hfe^{-/-}$ mice exhibit increased fatty acid oxidation and are hypermetabolic. The decreased glucose oxidation in skeletal muscle is due to decreased pyruvate dehydrogenase (PDH) enzyme activity related, in turn, to increased expression of PDH kinase 4 (*pdk4*). Increased substrate recycling to liver contributes to elevated hepatic glucose production in the $Hfe^{-/-}$ mice.

CONCLUSIONS—Increased hepatic glucose production and metabolic inflexibility, both of which are characteristics of type 2 diabetes, may contribute to the risk of diabetes with excessive tissue iron.

Emerging data demonstrate that iron plays an important role in metabolic regulation and the pathophysiology of diabetes. Iron overload is common in type 2 diabetes (1–3). Conversely, iron depletion seems to be protective for the development of diabetes. Rats with iron-deficiency anemia are more insulin sensitive than controls (4), and phlebotomy improves insulin sensitivity and glycemia, both in nondiabetic subjects (5) and type 2 diabetic subjects with high ferritin (6). These studies suggest that iron plays an important role in the development of diabetes. However, the precise molecular mechanisms of iron-associated diabetes are not well understood.

The most commonly studied model for iron-associated diabetes is hereditary hemochromatosis (HH), a common autosomal recessive disorder with a prevalence of 0.5% in people of northern European ancestry (7,8). The majority of individuals with HH carry a mutation (C282Y) in the *HFE* gene resulting in nonexpression of HFE on the cell surface (9,10). Normal HFE protein is required for iron stimulation of the hepatic synthesis of hepcidin, a peptide that regulates iron absorption through the downregulation of iron channel ferroportin (11). Failure to downregulate ferroportin in hemochromatosis leads to unlimited iron entry into the circulation from duodenal cells and macrophages (12). This results in iron overload in most major organs, including liver and pancreas (13), although based on the pathogenesis of the disease, tissues with high ferroportin expression such as enterocytes and macrophages have decreased iron levels (14). Diabetes is part of the classic presentation of HH, and our group as well as others have recently determined that prevalence of diabetes in persons with HH over the age of 45 exceeds 20% (15,16). We also reported that a mouse model of hemochromatosis with targeted deletion of the *Hfe* gene ($Hfe^{-/-}$), leading to defects in iron handling and iron overload very similar to the human disease, exhibits oxidative stress in islets and decreased insulin-secretory capacity (17). These defects, however, are well compensated in $Hfe^{-/-}$ mice that exhibit supernormal glucose tolerance and increased glucose uptake in skeletal muscle (18). Diabetes in humans with HH usually occurs in the setting of obesity, wherein it has been hypothesized that the resultant insulin resistance cannot be compensated because of the insulin secretory defect (15).

Other conditions that might predispose to diabetes in states of iron overload, such as dysregulation of hepatic glucose production or changes in the capacity to metabolize different fuels, have not been examined. To better understand the role of iron in diabetes and metabolic regulation, we have further studied glucose and fatty acid metabolism in $Hfe^{-/-}$ mice. $Hfe^{-/-}$ mice exhibit a preference for fatty acid as well as increased gluconeogenesis. The increased hepatic glucose production and metabolic inflexibility (19), both of which are characteristic of type 2 diabetes, may contribute to the risk of diabetes with excessive tissue iron.

From the [1]Departments of Medicine and Biochemistry, University of Utah School of Medicine, Salt Lake City, Utah; and [2]Research Service, VA Medical Center, Salt Lake City, Utah.

Corresponding author: Donald A. McClain, donald.mcclain@hsc.utah.edu.

Received 26 April 2010 and accepted 20 September 2010. Published ahead of print at http://diabetes.diabetesjournals.org on 28 September 2010. DOI: 10.2337/db10-0593.

RESEARCH DESIGN AND METHODS

Mice with knockout of the *Hfe* gene (*Hfe*$^{-/-}$) (13) were bred onto the 129/SvEvTac and C57BL/6J genetic backgrounds for more than 10 generations. Normal chow (Harlan Teklad TD-8640) contained 4.5% of calories as fat and 0.33 g/kg of carbonyl iron. High-fat diet (Research Diets D12451) contained 45% calories from fat. Mice were fed for a period of 2 months, beginning at age 4–6 months. Procedures were approved by the Institutional Animal Care and Use Committee of the University of Utah.

Quantification of transcript levels by RT-PCR. Quantative RT-PCR was performed as described previously (16). Muscle RNA was extracted using the PureLink Micro-to-Midi Total RNA Purification System (Invitrogen, Carlsbad, CA) according to the manufacturer's protocol. First-strand cDNA synthesis was carried out using Superscript III reverse transcriptase (Invitrogen) according to the manufacturer's protocol. Real-time PCR was performed with a thermal cycler (LightCycler, Roche Diagnostics, Basel, Switzerland) as previously described (20). Primers were designed using Primer3 software (http://primer3.sourceforge.net). Quantification of cDNA products was accomplished by the LightCycler software. Messenger RNA levels of specific genes were normalized to the average of the cyclophilin and Rpl13a levels for the same sample.

Measurement of mitochondrial oxygen consumption in skeletal muscle. Oxygen consumption in isolated muscle mitochondria was measured using a fiber-optic oxygen sensor (Ocean Optics, Orlando, FL) as previously described (21). Hindlimb soleus muscles were suspended in 2.0 ml of 120 mmol/l KCl, 3 mmol/l HEPES, 5 mmol/l KH2PO4, 1 mmol/l EGTA and 1 mg/ml fatty acid free BSA, pH 7.2. Respiration assay was performed in a thermostated (25°C), water-jacketed, sealed glass chamber with constant magnetic stirring. Oxygen consumption rates were measured for the following substrates: 5 mmol/l glutamate + 2 mmol/l malate in the basal state (state 2), after the addition of 1 mmol/l ADP (to maximally stimulate the respiration, state 3), and in the presence of 1 μg/ml oligomycin to block ATP synthesis (state 4). Respiratory control ratios were calculated as the ratio of respiration rate in state 3 to that in state 4.

Glucose oxidation. Soleus muscles were weighed and put in 24-well plates containing 400-μl Krebs-Ringer bicarbonate buffer (2.8 mmol/l glucose, 2 mg/ml BSA, 10 mmol/l HEPES [pH 7.4], 5 mmol/l $NaHCO_3$, 2.2 mmol/l $CaCl_2$, 1.2 mmol/l $MgSO_4$-$7H_2O$, 1.2 mmol/l KH_2PO_4, 4.8 mmol/l KCl, 126.2 mmol/l NaCl), pregassed for 30 min with 95% O_2/5% CO_2. Next, 3 μCi of [U-^{14}C] glucose were added to each well for 2 h at 37°C. Glucose oxidation was quantified by measuring $^{14}CO_2$ release, trapped by paper membranes soaked with hyamine hydroxide. Background release from a well containing no tissue was subtracted.

Hearts were perfused in the working mode and glucose oxidation determined as previously described (22).

Palmitate oxidation. Palmitate oxidation by soleus muscle was assayed as previously described (23,24) in 500-μl Krebs-Ringer bicarbonate buffer containing 1% fatty-acid free BSA, 1 mmol/l carnitine, and 5 μCi of [9,10-^{3}H] palmitate. Background ^3H_2O release measured in a well without tissue was subtracted from experimental values.

Indirect calorimetry. Mice age 6 to 8 months old were studied for 3 consecutive days in a four-chamber open-circuit Oxymas system (CLAMS; Columbus Instruments, Columbus, OH) to measure oxygen consumption and carbon dioxide production.

Hyperinsulinemic euglycemic clamp studies. Studies were performed in weight-matched nonsedated mice as described (25). The jugular vein was catheterized under avertin anesthesia, and using Micro-renathane tubing (Braintree Scientific, MRE 025). The animals were allowed to recover for 48 h before undergoing the clamp procedure. Mice were fasted overnight and transferred to a standard mouse housing cage with a tether arm attached to the catheter. A dual infusion pump (pump 33, Harvard Apparatus) was used to infuse insulin at a constant flow rate with no priming dose. A solution of 50% dextrose was infused at a variable rate to maintain a target value of 100–150 mg/dl and held at that level for 60 min. We also infusted [^{3}H]glucose at a constant rate (0.1μCi/min). Glucose was measured using 3 μl of tail vein blood at 10-min intervals using a tail clip and glucometer (Glucometer Elite, Bayer, Tarrytown, NY). Insulin levels did not differ between the groups, and we also determined that there was no change in insulin clearance in *Hfe*$^{-/-}$ mice as determined from C-peptide/insulin ratios (not shown).

Pyruvate dehydrogenase activity. Pyruvate dehydrogenase (PDH) activity was examined as described before (26) using a radioactive-enzymatic method. Frozen skeletal muscle tissue was homogenized in a buffer containing 25 mmol/l HEPES (pH 7.4), 3 mmol/l EDTA, 5 mmol/l sodium dichloroacetate, 1 mmol/l N-{α}-tosyl-L-lysylchloromethane, 1 mmol/l ADP, 5 mmol/l dithiothreitol, 2 mmol/l $CaCl_2$, 5 mmol/l $MgCl_2$, and 25 mmol/l KF, supplemented with 1.5% Triton X-100 and 5 μmol/l leupeptin. Before the addition of assay buffer, aliquots of homogenate were incubated at 30°C for 30 min to allow dephosphorylation and activation of PDH. Active PDH were determined in a reaction mixture containing 50 mmol/l HEPES (pH 7.4), 0.4 mmol/l thiamine pyrophosphate, 0.4 mmol/l CoA, 2 mmol/l dithiothreitol, 5 mmol/l NAD+, and 5 mmol/l $MgCl_2$, supplemented with 0.17% Triton X-100, 5 units/ml dihydrolipoamide reductase (E3), 20 μl of homogenate, and 2 μCi [1-^{14}C]-pyruvate. The PDH reaction yielding acetyl-CoA + CO_2 was performed at 30°C for 7 min before termination of the reaction by the addition of 2 mol/l acetic acid in 2% SDS. The $^{14}CO_2$ released from the PDH reaction was trapped by paper membranes soaked with hyamine hydroxide and quantified with a scintillation counter (Beckman Coulter). PDH activity was expressed as nmol · min^{-1} · mg tissue^{-1}.

Measurement of serum lipids and tissue pyruvate, lactate, and glycogen. Age-matched (6–8 month) male mice were killed. Serum triglycerides and free fatty acids were measured using assay kits from Sigma (St. Louis, MO) and Roche (Penzburg, Germany), respectively. Tissue was collected and tissue homogenates were used to assess pyruvate and glycogen levels. Pyruvate and lactate were measured by assay kits (Biovision, Mountain View, CA). Liver glycogen was measured as previously described (23).

Pyruvate tolerance testing. Blood glucose was measured with a glucometer in fasted mice before and after intraperitoneal injection of sodium pyruvate (2 mg/g body weight).

Western blotting for ferritin, AMPK, Akt, IRS2, and ACC. Hind-limb muscle was collected and tissue homogenates were prepared for Western blot analysis. Levels of total and/or phosphorylated proteins were detected by immunoblotting using the following antibodies: Acetyl-CoA carboxylase (Ser79) (Cell Signaling Technology, Danvers, MA), AMPK (Thr172) (Cell Signaling Technology), ferritin (Abcam, Cambridge, MA), Akt (Cell Signaling Technology), and IRS2 (Abcam). Signals quantified by densitometry were normalized to glyceraldehyde-3-phosphate dehydrogenase (GAPDH) levels (Santa Cruz Biotechnology, Santa Cruz, CA) or, in the case of phosphoproteins, to the total levels of the same protein.

Statistical procedures. Descriptive statistics are represented as average ± SEM. A two-tailed Student *t* test was used to compare the differences between groups.

RESULTS

Skeletal muscle is iron overloaded in Hfe$^{-/-}$ mice. As previously shown for other tissues (13,27), skeletal muscle in *Hfe*$^{-/-}$ mice is iron overloaded, with a 2.3-fold increase in ferritin compared with muscle of wild-type mice of the same strain (129SvEvTac, 129) as detected by Western blotting ($P < 0.01$, Fig. 1*A*). We have reported that nonheme iron is also elevated in *Hfe*$^{-/-}$ muscle (18).

Decreased glucose oxidation but relatively increased fatty acid oxidation in skeletal and cardiac muscle from Hfe$^{-/-}$ mice. We previously demonstrated that *Hfe*$^{-/-}$ mice exhibited increased muscle glucose uptake (18). To further study the metabolic fate of absorbed glucose, glucose oxidation was measured in skeletal and cardiac muscle. Isolated soleus muscle from 129 *Hfe*$^{-/-}$ mice exhibited a 33% decrease in glucose oxidation compared with wild type (Fig. 1*B*, $P = 0.05$). Similar results were obtained in isolated working hearts (Fig. 1*B*, $P < 0.005$). The decreased glucose oxidation, despite elevated glucose uptake in muscle, are manifest by increased lactate levels. We previously reported that lactate fluxes and serum lactate were elevated in *Hfe*$^{-/-}$ mice (18), and we have verified that tissue lactate levels are also increased by 46% in *Hfe*$^{-/-}$ muscle (9.1 ± 0.9 μg lactate/mg protein in wild-type muscle compared with 13.3 ± 1.1 μg/mg in *Hfe*$^{-/-}$ muscle, $N = 7$, $P = 0.01$, not shown).

We then measured fatty acid oxidation in isolated soleus muscle. *Hfe*$^{-/-}$ mice on the 129 or the diabetes- and obesity-prone C57BL/6J (C57) backgrounds demonstrated similar level of palmitate oxidation as determined by measuring ^3H_2O release from ^{3}H palmitate (Fig. 1*C*). However, in the setting of the decreased glucose oxidation, this represents a 47% increase in the ratio of fatty acid to glucose oxidation in the *Hfe*$^{-/-}$ compared with wild-type mice (Fig. 1*D*, $P < 0.01$). A relative increase in fatty acid oxidation is supported by decreased serum triglycer-

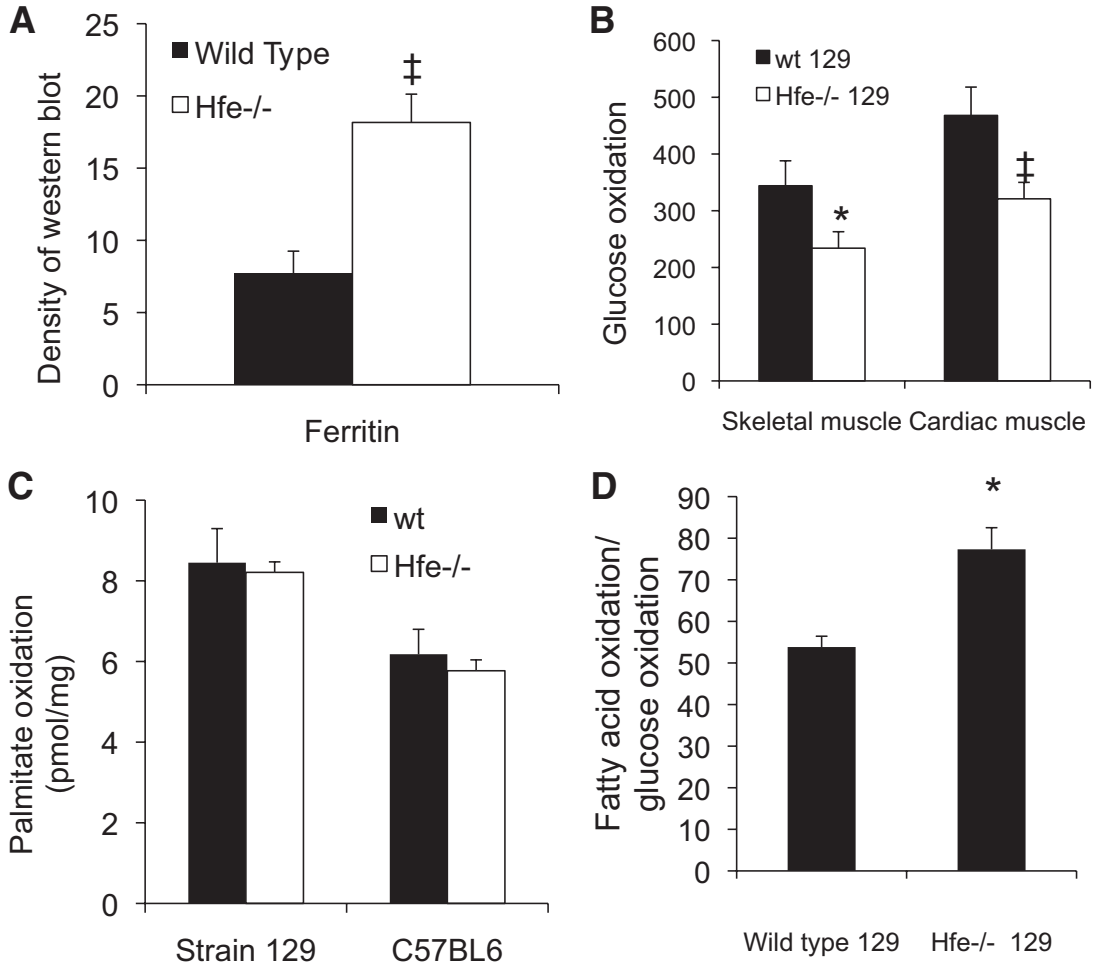

FIG. 1. Decreased glucose oxidation and relative preference for fatty acid oxidation in iron-overloaded muscle of wild-type and *Hfe*$^{-/-}$ mice on normal chow. *A*: Quantitation of Western blots for skeletal muscle ferritin in wild-type and *Hfe*$^{-/-}$ mice on the 129SvEvTac background (5/group). *B*, left side: Soleus muscle from 6- to 8-month-old male 129SvEvTac wild type that was exposed to [C^{14}] glucose and 10 mmol/l insulin. Results are normalized to muscle weight and presented as cpm/mg (P* < 0.05). *B*, right side: Glucose oxidation was also determined in hanging working hearts. *C*: Fatty acid oxidation in isolated soleus muscles was determined as release of $^{3}H_2O$ from labeled palmitate. (*N* = 7–8 pairs of muscles/group for each strain, presented as pmol palmitate per mg protein). *D*: Ratio of fatty acid oxidation to glucose oxidation (from data in panels *A* and *C*, 7 pairs of data per group). **P* < 0.01, ‡*P* < 0.01.**

ides in the *Hfe*$^{-/-}$ mice (52.3 ± 5.3 mg/dl in wild-type compared with 31.5 ± 8.6 mg/dl in *Hfe*$^{-/-}$ mice, N = 6/group, $P < 0.05$) and a trend toward decreased serum free fatty acids (0.061 ± 0.03 mmol/l in wild-type compared with 0.056 ± 0.025 mmol/l in *Hfe*$^{-/-}$ mice, $P = 0.18$).

There was no evidence of a change in glycogenolysis insofar as muscle glycogen levels did not differ between wild-type and *Hfe*$^{-/-}$ mice (10.6 ± 1.6 mg/g muscle in type compared with 8.3 ± 2.2 mg/g in *Hfe*$^{-/-}$ mice, N = 7/group, $P = 0.22$).

Modestly decreased mitochondrial respiration, increased PDH kinase 4 mRNA and decreased PDH activity in Hfe$^{-/-}$ muscle. To determine if decreased mitochondrial function contributed to the decreased glucose oxidation, mitochondrial function was analyzed by measuring oxygen consumption by permeabilized muscle fibers. Compared with wild-type mice, mitochondria from *Hfe*$^{-/-}$ soleus muscle exhibited only modestly decreased mitochondrial respiration. Under glutamate/malate-supported respiration, states 2, 3, and 4 respiration were apparently reduced by 19% ($P = 0.05$), 8.5% ($P = 0.22$), and 12.4% ($P = 0.13$), respectively (Fig. 2). ATP production also trended lower in *Hfe*$^{-/-}$ mice (16%), although not statistically significantly (not shown, $P = 0.31$). Mitochondrial density, as assessed by the ratio of mitochondrial to nuclear DNA, did not differ between wild-type and *Hfe*$^{-/-}$ mice (0.36 ± 0.06 vs. 0.32 ± 0.06 arbitrary units, respectively, $P = 0.68$).

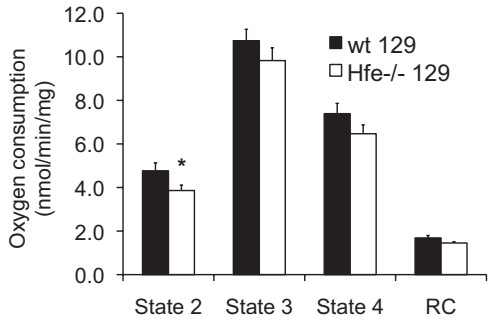

FIG. 2. Mitochondrial oxygen consumption in skeletal muscle of wild-type and *Hfe*$^{-/-}$ mice (129SvEvTac background). Mitochondrial oxygen consumption was determined in saponin-permabilized soleus muscle fibers. (*N* = 15–16 fibers/group. Statistical significance for differences by *t* test: state 2, **P* = 0.05; state 3, *P* = 0.22; state 4, *P* = 0.13; respiratory control ratio [RC], *P* = 0.46).

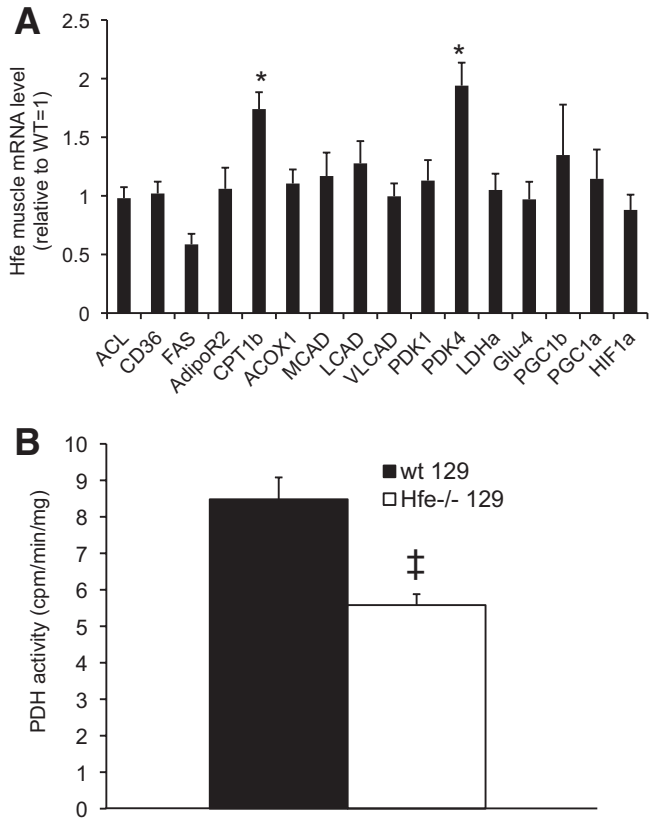

FIG. 3. Mechanism for decreased glucose oxidation in skeletal muscle of wild-type and *Hfe*$^{-/-}$ mice: Increased *Pdk4* and *cpt1b* mRNA, and decreased pyruvate dehydrogenase (PDH) activity. *A*: Expression of candidate genes in muscle of *Hfe*$^{-/-}$ mice and wild-type mice (129SvEvTac background) on normal chow, quantitated by RT-PCR (cDNA from seven mice per group, **P* < 0.05). *B*: Soleus muscle PDH activity assayed in vitro in wild-type and *Hfe*$^{-/-}$ mice (*N* = 5/group, ‡*P* < 0.005).

Hfe$^{-/-}$ mice, candidate gene expression was assessed in muscle using quantitative RT-PCR (Fig. 3*A*). Carnitine palmitoyl transferase b (*Cpt1b*) mRNA was increased by 74% and *Pdk4* mRNA by 94% in *Hfe*$^{-/-}$ mice compared with wild-type mice ($P < 0.05$). Fatty acid synthase mRNA was decreased by 41% in the *Hfe*$^{-/-}$ mice, although this difference did not reach statistical significance ($P = 0.08$). Transcripts of several other genes involved in nutrient transport or metabolism (*Acl*, *Cd36*, *Acox1*, *Mcad*, *Lcad*, *Pdk1*, *Ldh α*, *Glut4*, and *Hif1α*) did not differ. Because *Pdk4* and *Cpt1b* are PPARδ targets, we also measured PPARδ mRNA levels, but PPARδ did not differ between wild-type and *Hfe*$^{-/-}$ mice (7% decrease in *Hfe*$^{-/-}$ mice, $P = 0.48$, not shown).

The change in *pdk4* mRNA possibly explains decreased glucose oxidation because PDH kinase 4 (PDK4) phosphorylates and inhibits PDH, inhibiting pyruvate entry into the trichloroacetic acid; tricarboxylic acid (TCA) cycle (28). We therefore assessed the active fraction of PDH in soleus muscle, which was decreased by 34% in *Hfe*$^{-/-}$ compared with wild-type soleus muscle (Fig. 3*B*, $P < 0.001$). Total PDH activity did not differ between the two strains (18% increase in *Hfe*$^{-/-}$ mice, $P = 0.45$, not shown).

Increased fatty acid oxidation, increased oxygen consumption, and decreased respiratory exchange ratio in Hfe$^{-/-}$ mice on a high-fat diet. Fatty acids are relatively preferred as a fuel in muscle of *Hfe*$^{-/-}$ mice on a normal (high carbohydrate) chow diet. We therefore examined fatty acid oxidation in muscle of *Hfe*$^{-/-}$ mice on a high-fat diet, and in this case, isolated soleus muscle from *Hfe*$^{-/-}$ mice demonstrated an absolute increase in the capacity for fatty acid oxidation compared with wild type (Fig. 4*A*, $P < 0.05$). Consistent with their roles in regulating fatty acid oxidation, levels of pAMPK and pACC were increased in skeletal muscle of *Hfe*$^{-/-}$ mice on high fat (Fig. 4*B* and *C*).

The preference for fatty acid oxidation in *Hfe*$^{-/-}$ mice on a high-fat diet was confirmed in studies of mice in metabolic chambers. *Hfe*$^{-/-}$ mice on a high-fat diet exhibited significant increases in oxygen consumption (Fig. 4*D*) and heat production (Fig. 4*E*) compared with wild type. These were not specific to mouse strain, as the differences were significant for mice on either the 129 or C57Bl6 backgrounds. *Hfe*$^{-/-}$ mice on the high-fat diet also had significantly lower respiratory exchange ratios (Fig. 4*F*). Differences between *Hfe*$^{-/-}$ and wild type in heat production and respiratory exchange ratios were not apparent in mice fed the predominantly carbohydrate normal chow (not shown). In fact, *Hfe*$^{-/-}$ mice on both the 129 and C57 genetic backgrounds have lower oxygen consumption rates on high carbohydrate chow (25%, $P < 0.05$, not shown), consistent with their decreased glucose oxidation rates on the same diet (Fig. 1*B*).

Increased hepatic glucose output in Hfe$^{-/-}$ mice. To better understand the overall fuel economy in the *Hfe*$^{-/-}$ mice, we next measured hepatic glucose output (HGO) by means of the hyperinsulinemic euglycemic clamp. HGO was suppressed at maximal 10 mU/kg/min insulin in both wild-type and *Hfe*$^{-/-}$ mice (not shown), but at submaximal 5 mU/kg/min insulin, HGO was increased by 4.5-fold in *Hfe*$^{-/-}$ mice on normal chow and 1.7-fold on high fat (Fig. 5*A*, $P < 0.001$). The increased HGO did not appear to stem from an overall stimulation of the pathway for gluconeogenesis, as the mRNAs for phosphoenolpyruvate carboxykinase (PEPCK) and glucose-6-phosphatase (G6Pase) were not increased in livers of *Hfe*$^{-/-}$ mice (Fig. 5*B*). Consistent with this lack of upregulation of gluconeogenic enzymes, pyruvate tolerance testing revealed no difference in glucose production between wild-type and *Hfe*$^{-/-}$ mice (Fig. 5*C*). The increased HGO also did not stem from insulin resistance or insulin deficiency: We previously reported that glucose disposal determined by glucose clamp is elevated in *Hfe*$^{-/-}$ mice on normal chow at submaximal but not maximal glucose (18), and glucose disposal also trended toward an increase in the *Hfe*$^{-/-}$ mice on high fat compared with wild type (157 ± 36 vs. 95 ± 10 mg/kg/min, $P = 0.13$, not shown). Furthermore, hepatic insulin signaling was augmented in the *Hfe*$^{-/-}$ mice on normal chow. Fasted mice exhibited a 1.6-fold increase in phosphorylated Akt (pAkt) and a 2.3-fold increase in tyrosine phosphorylation of insulin receptor substrate-2 (pIRS2) (Fig. 5*D* and *E*, $P < 0.05$ for both). The source of the higher HGO also did not appear to be increased glycogenolysis, as hepatic glycogen levels were increased by 65.7% in *Hfe*$^{-/-}$ mice compared with wild-type mice (Fig. 5*F*, $P < 0.05$). Pyruvate levels were increased by 32% in livers of *Hfe*$^{-/-}$ mice (Fig. 5*F*, $P < 0.01$). Unlike the case in skeletal muscle, however, in liver there was no evidence for a decrease in pyruvate entry into mitochondrial oxidative pathways. Levels of *Pdk1* and *Pdk2* were in fact significantly lower in the *Hfe*$^{-/-}$ liver, which would favor increased PDH activity and decreased pyruvate levels; *Pdk's 3 and 4* were undetectable. The mRNA for pyruvate carboxylase (PCX) which catalyzes pyruvate conversion to oxaloacetate for either gluconeogenesis or anaplerotic entry of pyruvate into the TCA cycle

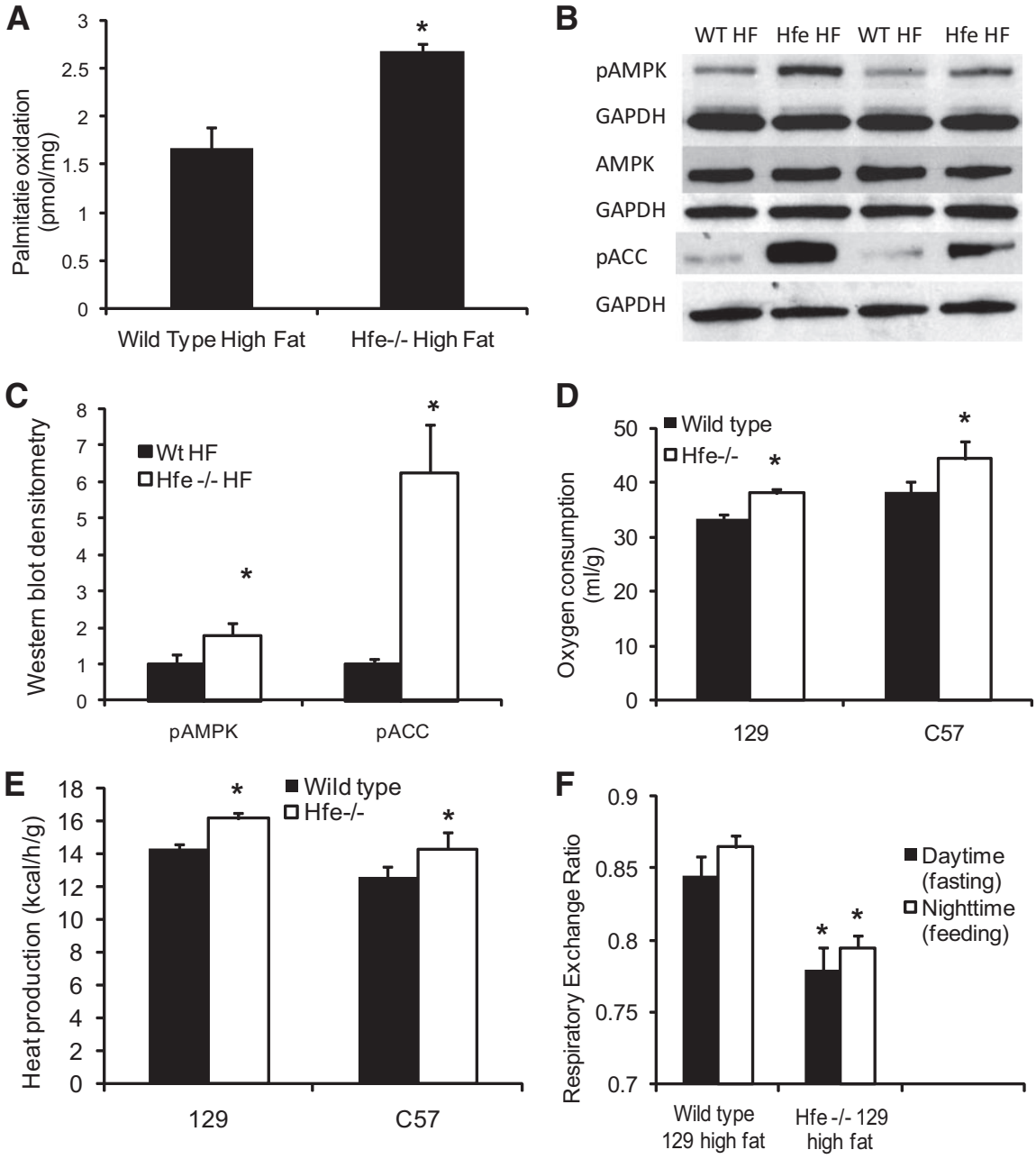

FIG. 4. *Hfe*$^{-/-}$ mice on a high-fat diet exhibit increased fatty acid oxidation and activation of AMPK in muscle, and hypermetabolism with a lower respiratory exchange ratio in vivo. Eight-month-old wild-type and *Hfe*$^{-/-}$ mice were fed a high-fat diet for 8 weeks before the study. *A*: Fatty acid oxidation in isolated soleus muscles of mice on the 129SvEvTac background was determined as release of ^3H_2O from labeled palmitate. (*N* = 5–6 pairs of muscles/group, presented as pmol palmitate per mg protein.) *B*: Muscle tissue from wild-type and *Hfe*$^{-/-}$ mice on the 129SvEvTac background was analyzed by Western blotting for activated pAMPK, total AMPK, and pACC, with GAPDH protein as a loading control shown for each gel. *C*: Densitometric data from four independent determinations per group were quantitated and normalized to GAPDH. *D–F*: Wild-type and *Hfe*$^{-/-}$ mice on either the 129SvEvTac or C57BL6/J genetic backgrounds were studied for 3 consecutive days by indirect calorimetry. *D*: Oxygen consumption. *E*: Heat production. *F*: Respiratory exchange ratio, the ratio of CO_2 production to O_2 consumption.

was slightly increased (25%, $P < 0.05$) in *Hfe*$^{-/-}$ mice compared with wild-type mice (Fig. 5*G*, $P < 0.05$). Both of these changes in liver would actually favor increased mitochondrial utilization of pyruvate in *Hfe*$^{-/-}$ liver. In sum, therefore, the data above suggest that the increased pyruvate and HGO largely result from increased peripheral cycling rather than decreased hepatic utilization.

DISCUSSION

Increased tissue iron levels are associated with diabetes, both in human hereditary hemochromatosis (HH) and in dietary iron overload (1,3,15,29,30). Although this is at least partially the result of decreased insulin secretion (15,17,27), tissue iron overload also results in significant changes in glucose metabolism in skeletal muscle (18). In that case, however, the effect of iron is to increase glucose uptake, a change that would be predicted to be protective of diabetes. To better understand the changes in overall fuel economy caused by iron that might contribute to diabetes, we have investigated muscle and hepatic carbohydrate and fatty acid metabolism in a mouse model with targeted deletion of the gene most commonly mutated in

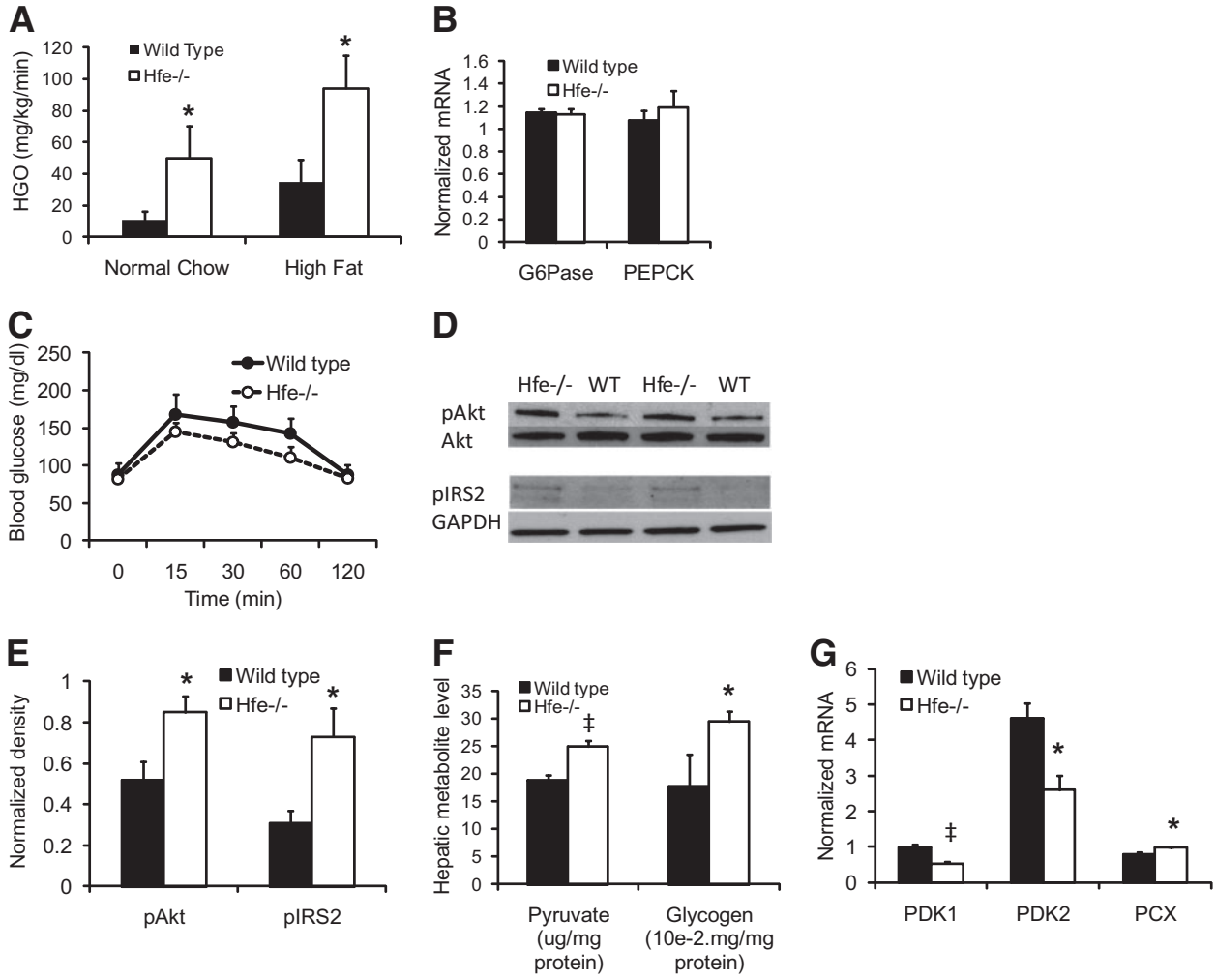

FIG. 5. Hepatic glucose metabolism in wild-type and *Hfe*$^{-/-}$ mice (129 strain) on normal chow. *A*: Hepatic glucose output (HGO) was determined by isotope dilution during euglycemic hyperinsulinemic clamps performed at submaximal (5 mU/kg/min) insulin infusion (N = 4–6 mice per group). *B*: Hepatic levels of mRNAs for glucose-6-phosphatase (G6Pase) and phosphoenolpyruvate carboxykinase (PEPCK) were determined by quantitative RT-PCR in liver. Results (N = 5–6/group) were normalized to cyclophilin A. *C*: Pyruvate tolerance testing of wild-type (N = 6) and *Hfe*$^{-/-}$ (N = 8) mice was performed by measuring blood glucose after injection of 2 mg pyruvate/g body weight. *D*: Phosphorylation of Akt and IRS2 were determined by Western blotting liver extracts from fasted wild-type and *Hfe*$^{-/-}$ mice on normal chow. *E*: Phosphorylation of Akt and IRS2 were normalized to total Akt and GAPDH, respectively, and quantitated by densitometry (N = 4 each). *F*: Levels of pyruvate and glycogen were determined in liver tissue (N = 4–6 per group). *P < 0.05, ‡P < 0.01. *G*: Hepatic levels of mRNAs for pyruvate dehydrogenases (PDK) 1 and 2 and pyruvate carboxylase (PCX) were determined by quantitative RT-PCR in liver. Results (N = 4–6 per group) were normalized to cyclophilin A.

human HH, *Hfe*. We show that *Hfe*$^{-/-}$ mice exhibit a shift in fuel preference from glucose to fatty acid oxidation in muscle. The decreased glucose oxidation in muscle is associated with increased pyruvate/lactate recycling to liver, as demonstrated in our previous metabolic flux studies (18), in Fig. 5, and by the increased hepatic glucose output. These combined effects may contribute to the increased prevalence of diabetes in individuals with HH.

Our results are consistent with the close coupling of metabolism to iron availability such as has been demonstrated in lower eukaryotes (31–33). The decreased glucose oxidation in skeletal muscle is due, at least in part, to decreased PDH activity. The mechanism is likely the observed increase in *Pdk4* mRNA, PDK4 activity being largely regulated at the transcriptional level (28). A candidate mediator for the regulation of *Pdk4* may be increased AMPK activity (34) that we previously reported in *Hfe*$^{-/-}$ mouse muscle (18). Other factors contributing to the decreased glucose oxidation include a modest degree of mitochondrial dysfunction and increased fatty acid oxidation (Randle effect) (35). The mitochondrial dysfunction in *Hfe*$^{-/-}$ muscle is likely, however, to be a relatively minor contributor given the increased capacity for fatty acid oxidation apparent in mice on high-fat diets.

The mechanism for the increased fatty acid oxidation is also likely multifactorial. We previously reported higher serum adiponectin levels in *Hfe*$^{-/-}$ mice (18) that would contribute to higher rates of fatty acid oxidation through increased AMPK activation and decreased ACC activity (36,37). Increased *Cpt1b* expression may also play a role, as might changes in malonyl-CoA, which were not assessed. Perhaps related to the current findings, mice overexpressing erythropoietin in muscle exhibit a similar phenotype to iron-overloaded mice, including increased fat oxidation, decreased glucose oxidation, and protection from diet-induced obesity, although tissue iron levels were not measured in that model (38). Insofar as iron sufficiency should facilitate unimpaired erythropoiesis, it would seem advantageous for an iron-sufficient mouse to shift to the more energy-efficient but oxygen-inefficient fuel source of fatty acids to make use of that full capacity for oxygen transport. Indeed, under the opposite condition of hyp-

oxia, fatty acid oxidation decreases, enzymes for fat metabolism downregulate, and glucose oxidation increases (39,40). Consistent with this proposed adaptive relationship between iron and fuel choice, *Hfe*$^{-/-}$ mice consume more oxygen and produce more heat when fat is available in the diet. A decreased ability to transition between utilization of carbohydrate and lipid fuel sources, so-called "metabolic inflexibility," is a characteristic of the metabolic syndrome and type 2 diabetes (19). Chronically increased fat oxidation, especially in the setting of decreased mitochondrial function, might also contribute to the accumulation of lipid products that have been implicated in the pathogenesis of diabetes (41). Whether these pathways contribute to increased diabetes risk in human hemochromatosis, however, is unknown.

The data are most consistent with the source of the increased hepatic glucose production being increased recycling of lactate and pyruvate, as was also previously documented by isotopomer analysis of the fate of 1,2[^{13}C]glucose (18). It appears that this increase in hepatic glucose production is mainly substrate driven as the levels of mRNA for gluconeogenic enzymes were not increased (Fig. 5*B*) and glucose production from exogenous pyruvate was not enhanced (Fig. 5*C*). The data also do not support changes in insulin signaling as the underlying cause of the phenotype. We previously demonstrated no change in basal or insulin-stimulated (in vivo) pAkt in skeletal muscle (18), and herein we shown that the increased hepatic glucose production occurs in the face of paradoxically increased insulin signaling in liver (Fig. 5*D* and E). Why insulin signaling is upregulated is not known. Levels of the insulin-sensitizing adipokine have been shown to be elevated in *Hfe*$^{-/-}$ mice (18), but other unknown factors may also contribute, including compensation for decreased insulin levels (17) or decreased inflammatory signaling in macrophages based on their lower iron content (42). Why this increased insulin signaling does not translate to decreased levels of gluconeogenic enzymes is unclear and is under investigation.

In sum, we have shown here and in previous work that the diabetes risk engendered by iron operates not only through its toxic effects on β cells mediated by increased oxidative stress and mitochondrial dysfunction. Rather, iron also exerts regulatory effects on metabolism and fuel choice. Iron overloaded skeletal muscle demonstrates decreased glucose oxidation and increased fatty acid oxidation. Liver of *Hfe*$^{-/-}$ mice exhibits increased glucose output, with the patterns of hepatic gene regulation and metabolite levels suggesting that the gluconeogenesis is largely substrate-driven and results from the altered fuel choice in muscle. These findings should help elucidate the association between iron and diabetes, not only in hemochromatosis, but also in nonhemochromatotic individuals with the metabolic syndrome or type 2 diabetes associated with dietary iron excess.

ACKNOWLEDGMENTS

This work was supported by the National Institutes of Health (DK-81842 [D.A.M.] and HL73167 [E.D.A.]), the Research Service of the Veterans Administration, and the University of Utah Center for Clinical and Translational Research (UL1-RR025764).

No potential conflicts of interest relevant to this article were reported.

J.H. wrote the manuscript and researched data. D.J., B.L., M.S., and J.S. researched data. E.D.A. researched data and contributed to discussion. D.A.M. wrote the manuscript and reviewed/edited the manuscript.

Parts of this study were presented in abstract form at the 70th Scientific Sessions of the American Diabetes Association, Orlando, Florida, 25–29 June 2010.

REFERENCES

1. Fernandez-Real JM, Lopez-Bermejo A, Ricart W. Cross-talk between iron metabolism and diabetes. Diabetes 2002;51:2348–2354
2. Forouhi NG, Harding AH, Allison M, Sandhu MS, Welch A, Luben R, Bingham S, Khaw KT, Wareham NJ. Elevated serum ferritin levels predict new-onset type 2 diabetes: results from the EPIC-Norfolk prospective study. Diabetologia 2007;50:949–956
3. Ford ES, Cogswell ME. Diabetes and serum ferritin concentration among U.S. adults. Diabetes Care 1999;22:1978–1983
4. Borel MJ, Beard JL, Farrell PA. Hepatic glucose production and insulin sensitivity and responsiveness in iron-deficient anemic rats. Am J Physiol 1993;264:E380–E390
5. Facchini FS. Effect of phlebotomy on plasma glucose and insulin concentrations. Diabetes Care 1998;21:2190
6. Fernandez-Real JM, Penarroja G, Castro A, Garcia-Bragado F, Hernandez-Aguado I, Ricart W. Blood letting in high-ferritin type 2 diabetes: effects on insulin sensitivity and β-cell function. Diabetes 2002;51:1000–1004
7. Edwards C. Hemochromatosis. In *Wintrobe's Clinical Hematology*. Lee GR FJ, Lukens J, Paraskevas F, Greer JP, Rodgers GM, Eds. Baltimore, MD, Williams & Wilkins, 1999, p. 1056–1070
8. Scriver CR, Beaudet AL, Sly WS, Valle D, Bothwell TH, Charlton RW, Motulsky AG. (1995) Haemochromatosis. In The metabolic and molecular basis of inherited disease. Eds Scriver CR, Beaudet AL, Sly WS, Valle D. McGraw-Hill, New York, pp 2237–2269
9. Feder JN, Gnirke A, Thomas W, Tsuchihashi Z, Ruddy DA, Basava A, Dormishian F, Domingo R Jr, Ellis MC, Fullan A, Hinton LM, Jones NL, Kimmel BE, Kronmal GS, Lauer P, Lee VK, Loeb DB, Mapa FA, McClelland E, Meyer NC, Mintier GA, Moeller N, Moore T, Morikang E, Wolff RK. A novel MHC class I-like gene is mutated in patients with hereditary haemochromatosis. Nat Genet 1996;13:399–408
10. Feder JN, Tsuchihashi Z, Irrinki A, Lee VK, Mapa FA, Morikang E, Prass CE, Starnes SM, Wolff RK, Parkkila S, Sly WS, Schatzman RC. The hemochromatosis founder mutation in HLA-H disrupts β2- microglobulin interaction and cell surface expression. J Biol Chem 1997;272:14025–14028
11. Nemeth E, Roetto A, Garozzo G, Ganz T, Camaschella C. Hepcidin is decreased in TFR2-hemochromatosis. Blood 2004;105:1803–1806
12. Nemeth E, Tuttle MS, Powelson J, Vaughn MB, Donovan A, Ward DM, Ganz T, Kaplan J. Hepcidin regulates cellular iron efflux by binding to ferroportin and inducing its internalization. Science 2004;306:2090–2093
13. Zhou XY, Tomatsu S, Fleming RE, Parkkila S, Waheed A, Jiang J, Fei Y, Brunt EM, Ruddy DA, Prass CE, Schatzman RC, O'Neill R, Britton RS, Bacon BR, Sly WS. HFE gene knockout produces mouse model of hereditary hemochromatosis. Proc Natl Acad Sci U S A 1998;95:2492–2497
14. Knutson MD, Oukka M, Koss LM, Aydemir F, Wessling-Resnick M. Iron release from macrophages after erythrophagocytosis is up-regulated by ferroportin 1 overexpression and down-regulated by hepcidin. Proc Natl Acad Sci U S A 2005;102:1324–1328
15. McClain DA, Abraham D, Rogers J, Brady R, Gault P, Ajioka R, Kushner JP. High prevalence of abnormal glucose homeostasis secondary to decreased insulin secretion in individuals with hereditary haemochromatosis. Diabetologia 2006;49:1661–1669
16. Hatunic M, Finucane FM, Brennan AM, Norris S, Pacini G, Nolan JJ. Effect of iron overload on glucose metabolism in patients with hereditary hemochromatosis. Metabolism 59:380–384
17. Cooksey RC, Jouihan HA, Ajioka RS, Hazel MW, Jones DL, Kushner JP, McClain DA. Oxidative stress, β-cell apoptosis, and decreased insulin secretory capacity in mouse models of hemochromatosis. Endocrinology 2004;145:5305–5312
18. Huang J, Gabrielsen JS, Cooksey RC, Luo B, Boros LG, Jones DL, Jouihan HA, Soesanto Y, Knecht L, Hazel MW, Kushner JP, McClain DA. Increased glucose disposal and AMP-dependent kinase signaling in a mouse model of hemochromatosis. J Biol Chem 2007;282:37501–37507
19. Storlien L, Oakes ND, Kelley DE. Metabolic flexibility. Proc Nutr Soc 2004;63:363–368
20. Cooksey RC, McClain DA. Transgenic mice overexpressing the rate-limiting enzyme for hexosamine synthesis in skeletal muscle or adipose tissue exhibit total body insulin resistance. Ann N Y Acad Sci 2002;967:102–111

21. Boudina S, Laclau MN, Tariosse L, Daret D, Gouverneur G, Bonoron-Adele S, Saks VA, Dos Santos P. Alteration of mitochondrial function in a model of chronic ischemia in vivo in rat heart. Am J Physiol Heart Circ Physiol 2002;282:H821–H831
22. Buchanan J, Mazumder PK, Hu P, Chakrabarti G, Roberts MW, Jeong Yun U, Cooksey RC, Litwin SE, Abel ED. Reduced cardiac efficiency and altered substrate metabolism precedes the onset of hyperglycemia and contractile dysfunction in two mouse models of insulin resistance and obesity. Endocrinology 2005;146:5341–5349
23. Cabrero A, Alegret M, Sanchez RM, Adzet T, Laguna JC, Vazquez M. Bezafibrate reduces mRNA levels of adipocyte markers and increases fatty acid oxidation in primary culture of adipocytes. Diabetes 2001;50:1883–1890
24. Muoio DM, MacLean PS, Lang DB, Li S, Houmard JA, Way JM, Winegar DA, Corton JC, Dohm GL, Kraus WE. Fatty acid homeostasis and induction of lipid regulatory genes in skeletal muscles of peroxisome proliferator-activated receptor (PPAR) α knock-out mice. Evidence for compensatory regulation by PPAR Δ. J Biol Chem 2002;277:26089–26097
25. Hebert LF Jr, Daniels MC, Zhou J, Crook ED, Turner RL, Simmons ST, Neidigh JL, Zhu JS, Baron AD, McClain DA. Overexpression of glutamine: fructose-6-phosphate amidotransferase in transgenic mice leads to insulin resistance. J Clin Invest 1996;98:930–936
26. Sterk JP, Stanley WC, Hoppel CL, Kerner J. A radiochemical pyruvate dehydrogenase assay: activity in heart. Anal Biochem 2003;313:179–182
27. Jouihan HA CP, Cooksey RC, Hoagland EA, Boudina S, Abel ED, Winge DR, McClain DA. Iron-mediated inhibition of mitochondrial manganese uptake mediates mitochondrial dysfunction in a mouse model of hemochromatosis. Mol Med 2008;14:98–108
28. Sugden MC, Holness MJ. Recent advances in mechanisms regulating glucose oxidation at the level of the pyruvate dehydrogenase complex by PDKs. Am J Physiol Endocrinol Metab 2003;284:E855–E862
29. Fleming DJ, Jacques PF, Tucker KL, Massaro JM, D'Agostino RB Sr, Wilson PW, Wood RJ. Iron status of the free-living, elderly Framingham Heart Study cohort: an iron-replete population with a high prevalence of elevated iron stores. Am J Clin Nutr 2001;73:638–646
30. Fleming DJ, Tucker KL, Jacques PF, Dallal GE, Wilson PW, Wood RJ. Dietary factors associated with the risk of high iron stores in the elderly Framingham Heart Study cohort. Am J Clin Nutr 2002;76:1375–1384
31. Treitel MA, Kuchin S, Carlson M. Snf1 protein kinase regulates phosphorylation of the Mig1 repressor in Saccharomyces cerevisiae. Mol Cell Biol 1998;18:6273–6280
32. Haurie V, Boucherie H, Sagliocco F. The Snf1 protein kinase controls the induction of genes of the iron uptake pathway at the diauxic shift in Saccharomyces cerevisiae. J Biol Chem 2003;278:45391–45396
33. Webster KA. Evolution of the coordinate regulation of glycolytic enzyme genes by hypoxia. J Exp Biol 2003;206:2911–2922
34. Jager S, Handschin C, St-Pierre J, Spiegelman BM. AMP-activated protein kinase (AMPK) action in skeletal muscle via direct phosphorylation of PGC-1α. Proc Natl Acad Sci U S A 2007;104:12017–12022
35. Randle PJ, Garland PB, Hales CN, Newsholme EA. The glucose fatty-acid cycle. Its role in insulin sensitivity and the metabolic disturbances of diabetes mellitus. Lancet 1963;1:785–789
36. Yamauchi T, Kamon J, Minokoshi Y, Ito Y, Waki H, Uchida S, Yamashita S, Noda M, Kita S, Ueki K, Eto K, Akanuma Y, Froguel P, Foufelle F, Ferre P, Carling D, Kimura S, Nagai R, Kahn BB, Kadowaki T. Adiponectin stimulates glucose utilization and fatty-acid oxidation by activating AMP-activated protein kinase. Nat Med 2002;8:1288–1295
37. Tomas E, Tsao TS, Saha AK, Murrey HE, Zhang Cc C, Itani SI, Lodish HF, Ruderman NB. Enhanced muscle fat oxidation and glucose transport by ACRP30 globular domain: acetyl-CoA carboxylase inhibition and AMP-activated protein kinase activation. Proc Natl Acad Sci U S A 2002;99:16309–16313
38. Hojman P, Brolin C, Gissel H, Brandt C, Zerahn B, Pedersen BK, Gehl J. Erythropoietin over-expression protects against diet-induced obesity in mice through increased fat oxidation in muscles. PLoS One 2009;4:e5894
39. Holden JE, Stone CK, Clark CM, Brown WD, Nickles RJ, Stanley C, Hochachka PW. Enhanced cardiac metabolism of plasma glucose in high-altitude natives: adaptation against chronic hypoxia. J Appl Physiol 1995;79:222–228
40. Kennedy SL, Stanley WC, Panchal AR, Mazzeo RS. Alterations in enzymes involved in fat metabolism after acute and chronic altitude exposure. J Appl Physiol 2001;90:17–22
41. Koves TR, Ussher JR, Noland RC, Slentz D, Mosedale M, Ilkayeva O, Bain J, Stevens R, Dyck JR, Newgard CB, Lopaschuk GD, Muoio DM. Mitochondrial overload and incomplete fatty acid oxidation contribute to skeletal muscle insulin resistance. Cell Metab 2008;7:45–56
42. Wang L, Harrington L, Trebicka E, Shi HN, Kagan JC, Hong CC, Lin HY, Babitt JL, Cherayil BJ. Selective modulation of TLR4-activated inflammatory responses by altered iron homeostasis in mice. J Clin Invest 2009;119:3322–3328